


Article

# Assessing the Impacts of Extreme Precipitation Change on Vegetation Activity

Fengsong Pei <sup>\*</sup>, Yi Zhou  and Yan Xia

School of Geography, Geomatics and Planning, Jiangsu Normal University, Xuzhou 221116, China; yzhou@jsnu.edu.cn (Y.Z.); xiayan@jsnu.edu.cn (Y.X.)

\* Correspondence: fengsong.pei.jsnu@gmail.com

**Abstract:** Extreme climate events frequently have more severe effects on terrestrial vegetation activity than long-term changes in climate averages. However, changes in extreme climate events as well as their potential risk on vegetation activity are still poorly understood. By using the Middle and Lower Reaches of the Yangtze River (MLR-YR) in China as an example, this paper aims to understand the vegetation response to changes in extreme precipitation events from 1982 to 2012 using the maximum normalized difference vegetation index (NDVI) as an indicator. By applying extreme value theory (EVT), the potential risks of extreme precipitation events on vegetation activity were analyzed by conducting return period analysis. Results indicated that vegetation activity could be affected by extreme precipitation events, especially the combined effects of the frequency and intensity of precipitation extremes. For instance, vegetation activity could be enhanced in the regions with weakened intensity but increased occurrence of extreme precipitation events. In addition, we found potential risk of extreme precipitation events on vegetation activity from the results of precipitation extreme trend and return period analysis. These phenomena can be associated with the local occurrence of extreme precipitation events, different land cover types, and soil moisture cumulative effect on vegetation growth. This study stresses the importance of considering both current changes in and the potential risk of extreme precipitation events to understand their effects on vegetation activity.

**Keywords:** vegetation activity; extreme precipitation events; return period analysis; the middle and lower reaches of the Yangtze River



**Citation:** Pei, F.; Zhou, Y.; Xia, Y. Assessing the Impacts of Extreme Precipitation Change on Vegetation Activity. *Agriculture* **2021**, *11*, 487. <https://doi.org/10.3390/agriculture11060487>

Academic Editor: Francesco Primo Vaccari

Received: 6 April 2021  
Accepted: 23 May 2021  
Published: 24 May 2021

**Publisher's Note:** MDPI stays neutral with regard to jurisdictional claims in published maps and institutional affiliations.



**Copyright:** © 2021 by the authors. Licensee MDPI, Basel, Switzerland. This article is an open access article distributed under the terms and conditions of the Creative Commons Attribution (CC BY) license (<https://creativecommons.org/licenses/by/4.0/>).

## 1. Introduction

Global surface temperature rose by approximately 1.38~1.68 °C between 1850~1900 and 2006~2015 [1–3]. Under current conditions, extreme climate events are projected to be enhanced in future decades [4–6]. Extreme climate (weather) events refer to the occurrence of an event when a given meteorological variable is above (or below) a threshold near the upper (or lower) ends of the time series of its observed value [7,8]. Particularly, the effects of extreme climate events on terrestrial vegetation activity are more severe than that of long-term change in climate averages due to probable flooding, heatwaves and droughts [9–11].

As one of important climate extremes, extreme precipitation events exert complex effects on vegetation activity owing to the complexity of the precipitation extremes, diversified land cover types, etc. [12–14]. It is essential to detect the responses of vegetation activity to the changes in extreme precipitation events as well as their potential risk. In this paper, vegetation activity refers to the abilities of the terrestrial vegetation that interacts with surrounding environments, including photosynthesis and respiration [15]. In the past decades, Normalized Difference Vegetation Index (NDVI) and Leaf Area Index (LAI) have been proposed to reflect changes in vegetation activity. The NDVI is widely employed for its simplicity and long-term archives to facilitate the large-scale monitoring of terrestrial

vegetation activity [16,17]. As for extreme precipitation events, the European Climate Assessment (ECA) indices were developed to account for climate extremes, including temperature, precipitation and frost [18]. On this basis, many extreme climate indices were proposed by the Expert Team on Climate Change Detection and Indices (ETCCDI), which was employed in the fourth and fifth Intergovernmental Panel on Climate Change (IPCC) reports [19]. Tan et al. (2015) [20] analyzed the relationships between vegetation activity and precipitation extremes in the Poyang Lake Basin, China. They found significant negative correlations between NDVI and extreme precipitation indices (i.e., RX1day and RX5day) in summer and winter during 1982–2006. In addition, Cui et al. (2019) [21] found significant and negative correlations between extreme precipitation indices (i.e., R95p and R95) and annual mean NDVI during 1982–1994. However, no significant correlation was found between the two factors in the Yangtze River Basin over the period of 1982–2015. According to Zhao et al. (2018) [22], positive correlations could exist in the Loess Plateau in summer over the period 1982–2013 between vegetation change and precipitation extremes using NDVI, RX1day and RX5day as indicators. Utilizing a replicated regression experiment, Felton et al. (2018) [23] found that vegetation response to changes in the growing season precipitation may weaken or even shift owing to greater magnitudes of precipitation extremes. Luo et al. (2020) [24] assessed extreme climatic changes in Central Asia on a monthly scale and discussed their implications for vegetation. They found that vegetation activity is significantly and positively related to extreme precipitation and temperature intensity indices on a monthly scale. There remains uncertainty regarding the effect of extreme precipitation events on vegetation activity. In addition, past studies mainly explored the effect of historical characteristics of extreme precipitation events on vegetation activity by using existing extreme precipitation indices; limited attention was paid to the potential risk of extreme changes in precipitation on vegetation activity.

The Yangtze River, being the third longest river worldwide, is characterized by frequent occurrence of precipitation extremes. The middle and lower reaches of the Yangtze River (MLR-YR) cover many of the economically developed areas in China. By using the NDVI in the growing season as a proxy of vegetation activity, this paper aims to provide an improved understanding of vegetation sensitivity to extreme precipitation events at a regional scale by addressing both historical data and return period analysis. Extreme Value Theory (EVT) was developed to describe the characterization of extremes [25]. According to EVT, several methods were employed to deal with climate extremes, including Generalized Pareto Distribution (GPD) and Generalized Extreme Value (GEV) distribution [26,27]. To assess the potential risk of extreme precipitation events, this paper compared the two methods and fit them to observed records to estimate return levels at different return periods in the MLR-YR. Concretely, we analyzed the impacts of the frequency and intensity of extreme precipitation events on vegetation activity in the MLR-YR. We considered two measures of extreme precipitation events from the perspectives of frequency and intensity using extreme precipitation indices [19,28]. Furthermore, potential risks were preliminarily examined by comparing historical characteristics of extreme precipitation events with precipitation amounts in different return periods. This paper can contribute to understanding the vegetation response to the changes in extreme precipitation events and their potential risks.

## 2. Study Area and Data Sources

### 2.1. Study Area

The Yangtze River, being the third longest river in the world, is a storm-flood river with frequent storm-flood events. For instance, disastrous floods in the years 1954, 1998 and 2010 caused large losses in the economy and human life [29,30]. In this paper, the study area is distributed over the middle and lower reaches of the Yangtze River (MLR-YR). The MLR-YR lies between 102° E~122° E and 24° N~34° N, with a total area of 1,157,057 km<sup>2</sup>. It has many tributaries, including the Hanjiang River, Jianglingjiang River, Wujiang River, Xiangjiang River, Ganjiang River and Yuanjiang River (Figure 1). In addition, the average

annual temperature is 14~18 °C. Meanwhile, average annual precipitation ranges between 1000 mm and 1500 mm in this region. Owing to a typical subtropical monsoon climatic zone, the MLR-YR is characterized by a favorable environment for plant growth due to the concurrent occurrence of rainfall and heat energy in the same seasons. The major ecosystems in this region encompass evergreen broadleaf forest, croplands, grasslands, etc. In addition, the MLR-YR is one of the most economically developed regions in China. It is therefore among the important vulnerable zones owing to high exposure of population and economic assets to climatic extremes in China.

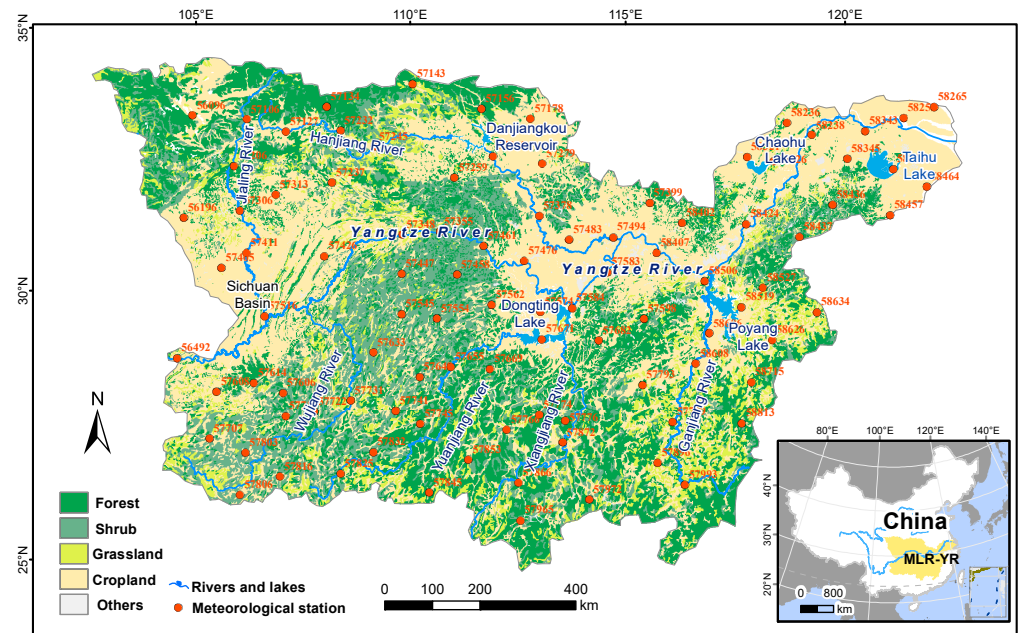


Figure 1. The location of the middle and lower reaches of the Yangtze River (MLR-YR).

2.2. Data and Preprocessing

The data used in this study includes daily precipitation datasets, NDVI datasets and land use/cover datasets in the MLR-YR. Daily precipitation data, which cover 1982–2012, were obtained from the Chinese Meteorological Data Service Center (CMDC). Time consistency and extremum validation were first inspected by the CMDC to ensure the data quality [31]. Furthermore, weather stations with suspicious and missing records were screened and eliminated when validating the data. A total of 97 stations, which are nearly evenly distributed in the study area (Figure 1), were then selected to analyze the change in extreme precipitation events in this region. Among the weather stations, a total of 28 stations are distributed in the lower reach of the Yangtze River Basin, with the rest of the stations in the middle reach of the Yangtze River Basin (Figure 1 and Table 1).

Table 1. Distribution of weather stations in the MLR-YR.

Data	Applicable Weather Stations	Natural Division	Main Tributaries	Main Lakes or Reservoir
Daily precipitation, 1982–2012	28 stations	The lower reach of the Yangtze River	Ganjiang River	Poyang Lake Taihu Lake Chaohu Lake
	69 stations	The middle reach of the Yangtze River	Xiangjiang River Yuanjiang River Wujiang River Jialingjiang River Hanjiang River	Dongting Lake Danjiangkou Reservoir

As to the NDVI data, the third generation Advanced Very High Resolution Radiometer (AVHRR) NDVI dataset (i.e., NDVI3g) was employed at a resolution of 1/12 degrees over the period 1982–2012. In detail, the AVHRR NDVI3g data were produced in the Global Inventory Monitoring and Modeling System (GIMMS) project to deal with deleterious effects of the first generation NDVI data (NDVIg), including orbital drift, calibration loss and volcanic eruptions [32]. The NDVI3g data were derived from the US National Aeronautics and Space Administration (NASA) Ames Ecological Forecasting Lab (<https://ecocast.arc.nasa.gov/> (accessed on 8 December 2019)). In addition, land use/cover data in 2005 were obtained at a spatial resolution of 500m from the Moderate Resolution Imaging Spectroradiometer (MODIS) product (MCD12Q1). Concretely, the MCD12Q1 data were downloaded from the NASA Land Processes Distributed Active Archive Center (LP DAAC), a part of NASA's Earth Observing System Data and Information System. Both the NDVI3g and the MCD12Q1 data were then aggregated into a resolution of 4 km × 4 km.

### 3. Methods

#### 3.1. The NDVI as a Proxy to Monitor the Vegetation Activity

In past decades, remote sensing was widely employed in monitoring terrestrial vegetation activity. Many vegetation indices, including Ratio Vegetation Index (RVI), NDVI and atmospherically resistant vegetation index (ARVI), were developed to reflect the changes in vegetation growth [33–36]. For instance, the third generation NDVI data from NOAA/AVHRR has advantages in capturing vegetation activities owing to the dramatic improvement of the data quality. The NDVI is defined as

$$\text{NDVI} = \frac{\text{NIR} - \text{RED}}{\text{NIR} + \text{RED}} \quad (1)$$

where *NIR* and *RED* represent surface reflectance in the near-infrared band and the red band of the satellite images, respectively.

To explicitly capture changes in vegetation activity, grid cells with annual mean NDVI less than 0.1 were masked out to exclude water, bare land and sparse vegetation in this study. We conducted three experiments to capture vegetation activity by analyzing the sensitivity of vegetation activity to maximum, average and minimum NDVI. Consequently, maximum NDVI in the growing season was found to capture changes of vegetation activity well [37]. A linear regression model was applied on the maximum NDVI to assess whether strengthened (or decreased) vegetation activity exists.

#### 3.2. The Peaks-Over-Threshold (POT) Approach and the Simple Indices of Extreme Precipitation Frequency (EPF) and Extreme Precipitation Intensity (EPI) to Analyze Extreme Precipitation Events

The POT approach is frequently used to analyze the changes in extreme climate events [38–43]. In addition, many climate extreme indices were recommended by the Expert Team on Climate Change Detection and Indices (ETCCDI). The Rnnmm refers to the annual count of days when daily precipitation amount exceeds a given threshold [44]. After empirically determining the thresholds of extreme precipitation events (i.e., daily precipitation at 99th percentiles), extreme precipitation frequency was analyzed using the simple index of extreme precipitation frequency, where  $P_1, P_2, \dots, P_d$  were independent random observations of a random variable, such as daily precipitation in a given period (e.g., one year). A simple index of extreme precipitation frequency (EPF) was calculated as

$$\text{EPF} = \sum_{j=1}^{365} \tau_{yd} \quad (2)$$

$$\tau_{yd} = \begin{cases} 1 & P_d \geq u \\ 0 & P_d < u \end{cases} \quad (3)$$

where  $\tau_{yd}$  is a conditional function that takes the value 1 if daily precipitation observation  $P_d$  on the day  $d$  in the year  $y$  exceeds the extreme precipitation threshold  $u$ . Otherwise,  $\tau_{yd}$  takes a value of zero, indicating non-occurrence of extreme precipitation events. If daily precipitation amount on several consecutive days exceeds the given threshold, it will be counted as a continuous extreme precipitation event. Further details about the EPF can be found in Pei et al. (2017) [28].

Given the discrete characteristics of the occurrence of extreme precipitation events, we fit the number of the extreme precipitation events to a conditional Poisson distribution. We then calculated the dispersion coefficient to check the reliability of the Poisson distribution. On this basis, a Poisson regression model was employed to detect the trend of extreme precipitation events [45–47]. That is, the amount of extreme precipitation events in the year  $y$  ( $N_y$ , equals to EPF) follows a conditional Poisson distribution with the occurrence rate ( $\lambda_y$ ), as follows:

$$P(N_y = k | \lambda_y) = \frac{e^{-\lambda_y} \lambda_y^k}{k!} [k = 0, 1, 2, \dots] \quad (4)$$

Generally, occurrence rate ( $\lambda_y$ ) is a non-negative random variable. For assessing the temporal trends of extreme precipitation events, the occurrence rate ( $\lambda_y$ ) in a given year ( $y$ ) was fit as a linear function of  $y$  (by a logarithmic link function), as follows:

$$\lambda_y = \exp(a + b \cdot y) \quad (5)$$

where  $a$  and  $b$  represent regression coefficients. If  $b$  is larger (or smaller) than zero at the 5% significance level according to the Wald test ( $p < 0.05$ ), then statistical evidence is found to support the presence of the increased (or decreased) occurrence of extreme precipitation events [46,47].

To analyze the changes in extreme precipitation intensity in the MLR-YR, the simple index of extreme precipitation intensity (EPI) was employed as a proxy of extreme precipitation intensity. In detail, the EPI is calculated as the ratio between the cumulative daily precipitation ( $P_{yd}$ , mm) and the number of extreme precipitation events in the year  $y$  ( $N_y$ ):

$$EPI = \left( \sum_{d=1}^{365} P_{yd} \right) / N_y \quad P_{yd} > u \quad (6)$$

where  $P_{yd}$  (mm) is the precipitation amount on the given day  $d$  in the year  $y$ ;  $u$  is the selected threshold to identify the extreme precipitation events. Further details about the EPI can be found in Pei et al. (2017) [28].

When evaluating temporal changes of extreme precipitation intensity ( $EPI_t$ ), a linear regression model was used to assess whether a statistically significant strengthened or decreased trend exists. In detail, we assumed that the  $EPI_t$  depends linearly on the time  $t$ :

$$EPI_t = \alpha + \beta \cdot T \quad (7)$$

where  $\alpha$  and  $\beta$  represent regression coefficients. According to the  $t$ -test ( $p < 0.05$ ), if  $\beta$  is different from zero at the 5% significance level, then statistical evidence is found in favor of the presence of the trends in the intensity of extreme precipitation events.

### 3.3. Assessment of Daily Precipitation Extremes for Different Return Periods

In this paper, the return period of daily precipitation extremes was analyzed to evaluate extreme precipitation risk on vegetation activity in the MLR-YR. A return period refers to the average recurrence interval of extreme climate events over an extended period based on historical data analysis [48]. Here return levels in different return periods were assessed using the GPD and the GEV.



As to the GPD approach, by comparing daily precipitation value with a given threshold, the approach detects whether extreme an precipitation event occurs. For a random variable  $x(x \geq u)$ , the cumulative probability function of the GPD is as follows:

$$(x) = \begin{cases} 1 - (1 + \frac{\xi(x-u)}{\sigma})^{-1/\xi}, \xi \neq 0 \\ 1 - \exp(-\frac{x-u}{\sigma}), \xi = 0 \end{cases} \tag{8}$$

where  $u$  represents the location parameter and  $\sigma$  and  $\xi$  are the scale and shape parameters, respectively. In past studies, different daily precipitation amounts were tested to determine the threshold of extreme precipitation events in the MLR-YR. The 95th and 99th percentile of daily precipitation amounts on rainy days were found to have a near-equidispersion coefficient in most stations from 1982 to 2012 [28]. Considering the NDVI extreme analysis only in the growing season, the location parameter was empirically determined as the daily precipitation amount of the 99th percentile of the cumulative frequency distribution on the rainy days in a given year in the MLR-YR.

In addition, probability weighted moments (PWMs) estimator was employed to determine the shape parameter ( $\hat{\xi}$ ) and the scale parameter ( $\hat{\sigma}$ ) for its lower uncertainty [49]. Concretely, the shape parameter ( $\hat{\xi}$ ) and the scale parameter ( $\hat{\sigma}$ ) of the GPD is determined using L-moments, as follows [50,51]:

$$\hat{\xi} = \frac{l_1}{l_2} - 2 \text{ and } \hat{\sigma} = (1 + \hat{\xi})l_1 \tag{9}$$

where  $l_1$  and  $l_2$  are the first two sample L-moments of random variable  $X$ . If  $m$  denotes the number of samples collected over many years and  $n$  is the total number of exceedances over the selected threshold  $u$ , mean crossing rate can then be estimated without bias as  $\lambda = \frac{n}{m}$ . For the Generalized Pareto Distribution, the number of exceedances in the year  $t$  is as follows:

$$\lambda_x = \lambda t(1 - F) \tag{10}$$

On this basis, taking  $(1 - F)$  from Equation (10), setting  $\lambda_x$  to unity, and setting  $t$  to  $T$ , the quantile  $x_T$ , which corresponds to the return level during a T-year return period, can be estimated as follows:

$$x_T = \begin{cases} u + \frac{\sigma}{\xi} [1 - (\lambda T)^{-\xi}] \text{ for } \xi \neq 0 \\ u + \sigma \ln(\lambda T) \text{ for } \xi = 0 \end{cases} \tag{11}$$

As to the Generalized Extreme Value (GEV) distribution, distribution function is defined according to Jenkinson [52], as follows:

$$(x) = \begin{cases} \exp(-(1 - \frac{\xi(x-u)}{\sigma})^{1/\xi}), \xi \neq 0 \\ \exp(-\exp(-\frac{x-u}{\sigma})), \xi = 0 \end{cases} \tag{12}$$

where  $u$  is the location parameter;  $\sigma$  is a scale parameter;  $\xi$  denotes shape parameter. For the quantile  $x_P$  of GEV distribution, with the return period  $T$ , the cumulated probability is given by  $F(x_P) = 1 - (1/T)$ , which results in [51,53] the following:

$$x_P = \begin{cases} u + \frac{\sigma}{\xi} [1 - (-\ln(1 - \frac{1}{T}))^\xi] \text{ for } \xi \neq 0 \\ u - \sigma \ln(-\ln(1 - \frac{1}{T})) \text{ for } \xi = 0 \end{cases} \tag{13}$$

### 3.4. Relationships between Vegetation Activity and extreme Precipitation Events

In this paper, maximum NDVI was composited by selecting the maximum NDVI in the growing season from many observations in a given year from 1982 to 2012. To examine the region’s vegetation responses to changes in extreme precipitation events, further analysis was conducted for the maximum NDVI. Concretely, interannual changes

of the maximum NDVI variable and the intensity and frequency of daily precipitation extremes were analyzed in the MLR-YR for the period 1982–2012 using linear regression and Poisson regression analyses, respectively. The spatial patterns of the frequency and intensity of daily precipitation extremes were analyzed by using inverse distance weighted (IDW) interpolation. Both regional averages and station-based analyses were further applied to the maximum NDVI variable and the frequency and intensity of daily precipitation extremes. Correlation analysis was conducted by meteorological stations to elucidate the relationships among the NDVI variables and the intensity/frequency of extreme precipitation events.

For assessing potential risks of extreme precipitation events on vegetation activity, observed precipitation in the MLR-YR was fit to extreme distributions (i.e., GPD and GEV). To evaluate the accuracy of the GPD and GEV, the return level for a 30-year return period was then estimated and compared with annual maximum precipitation that was extracted from the observed records in the MLR-YR from 1982 to 2012. Concretely, we first extracted two data series using daily precipitation records: annual maximum (AM) series and peak-over-threshold (POT) series. On this basis, we fit the GEV distribution to observed records using the *extRemes*-package in R software [54,55]. In addition, the POT series was fit to the GPD series using the POT package in R [54,56]. The results showed that the patterns of the return levels at a 30-year return period were similar between the GEV (not shown in this paper) and GPD simulations. In addition, the return level from GPD fitting was bigger than that from the GEV fitting. Specifically, observed maximum precipitation varied between 77 mm and 393 mm from 1982 to 2012 according to the meteorological-station-based observations. As to the projected precipitation amounts, the return level from GEV fitting varied between 71 mm and 295 mm. In addition, the return level from GPD fitting in the MLR-YR varied between 70 mm and 330 mm, which is close to that of the observed maximum precipitation. Thus, we chose the GPD to fit the return levels of extreme precipitation events in the MLR-YR from 1982 to 2012. Based on the GPD simulations for the return periods of 30 years, 50 years and 100 years, we preliminarily analyzed the potential risk of extreme precipitation events on vegetation activity by coupling historical changes of precipitation extremes with the precipitation changes in different return periods.

## 4. Results

### 4.1. Spatiotemporal Changes of Maximum NDVI and Precipitation Extremes

By using maximum NDVI in the growing season as a proxy, Figure 2 shows interannual changes of vegetation activity from 1982 to 2012 in the MLR-YR. Concretely, maximum NDVI varied between 0.73 and 0.79 in the past decades. In addition, slightly increasing trends of the maximum NDVI were found, at a rate of 0.01 units per decade ( $p = 0.000$ ). In particular, relatively low maximum NDVI was found in the years 1982, 1993, 1994, 2000 and 2005.

In addition, the changes in extreme precipitation events were analyzed in the MLR-YR from 1982 to 2012 from the perspectives of intensity and frequency. As shown in Figure 3, similar changes were found between extreme precipitation frequency and extreme precipitation intensity using the EPI and the EPF as indicators. Specifically, we found a significant increased trend in the extreme precipitation intensity, at a rate of  $0.169 \text{ mm day}^{-1} \text{ year}^{-1}$  ( $p = 0.045$ ). As to the extreme precipitation frequency, a slightly increased trend of  $0.004 \text{ day year}^{-1}$  was found in the past decades, albeit not significant ( $p = 0.481$ ). In particular, a relatively high extreme precipitation intensity was found in the years 1984, 1988, 1991, 1996, 1998 and 2010. Meanwhile, a frequent occurrence of extreme precipitation events could also be observed in the same periods.

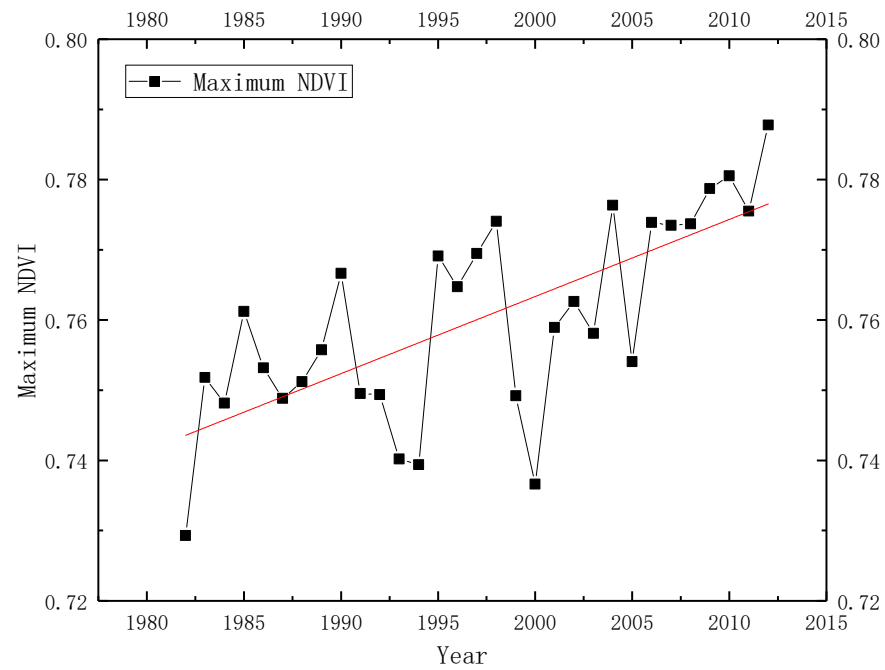


**Figure 2.** Temporal variations of maximum normalized difference vegetation index (NDVI) in the MLR-YR from 1982 to 2012.

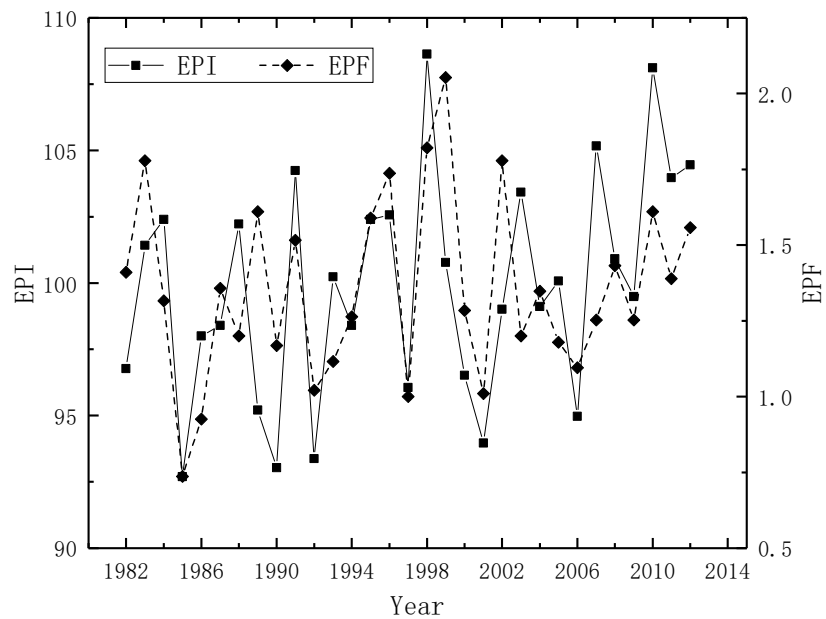


**Figure 3.** Temporal variations in the extreme precipitation intensity (EPI) and extreme precipitation frequency (EPF) in the MLR-YR from 1982 to 2012.

We further explored the spatial heterogeneities of the changes in the maximum NDVI. As shown in Figure 4a, the maximum NDVI showed an overall increased trend from 1982 to 2012 in the MLR-YR. However, decreased NDVI could be found locally, including the regions around Sichuan Basin.



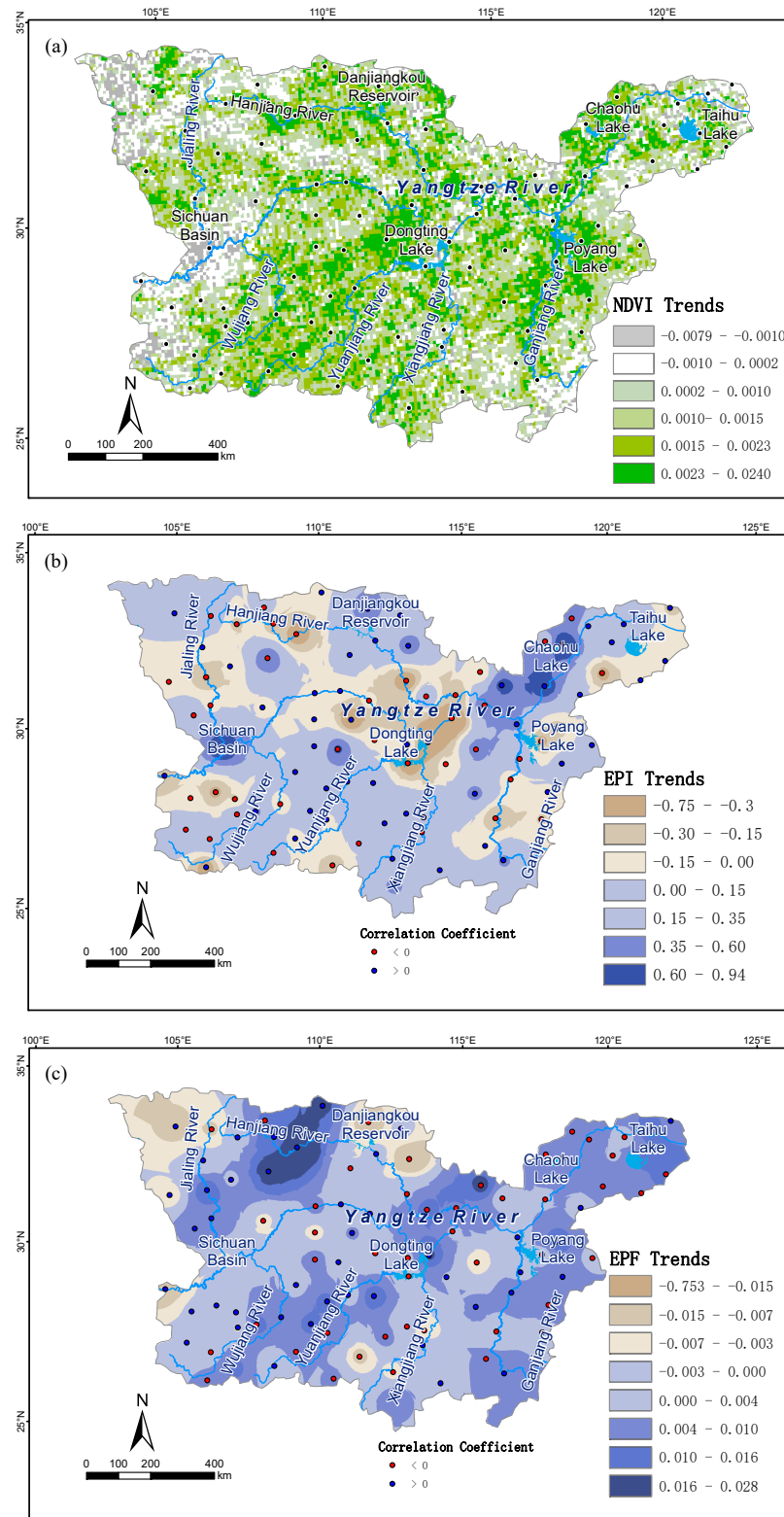


**Figure 4.** Spatial trends of (a) maximum NDVI, (b) EPI and (c) EPF in the MLR-YR from 1982 to 2012. Blue (red) points represents positive (negative) correlation between maximum NDVI and (b) EPI and (c) EPF.

In addition to temporal variations, changes in the two extreme precipitation indices were also spatially examined in the MLR-YR from 1982 to 2012. As shown in Figure 4b, the extreme precipitation intensity (EPI) showed an overall enhanced trend in the MLR-YR in

past decades. However, weakened extreme precipitation intensity could also be observed locally. For instance, the stations with weakened intensity of extreme precipitation events were distributed mainly around the Hanjiang River Basin and the Dongting-Changjiang and the Poyang-Changjiang regions. In conjunction with the changes in extreme precipitation intensity, increased occurrence of extreme precipitation events (EPF) could be found in most of the regions in the MLR-YR (Figure 4c). In particular, a remarkable increase in the extreme precipitation events could be found in the Hanjiang River Basin in past decades, especially in the regions around Wanyuan station (Station ID: 57237 in Figure 1), along the western parts of the Hanjiang River. In contrast, extreme precipitation frequency (EPF) was severely weakened in the regions in the northwestern Jialingjiang-Minjiang and Danjiangkou-Hanjiang in the northern MLR-YR. In addition, obvious concurrent enhancements of intensity and frequently of extreme precipitation events could also be found around the eastern parts of the MLR-YR.

#### 4.2. The Impacts of Extreme Precipitation Events on Vegetation Activity

We further analyzed the correlations between maximum NDVI and extreme precipitation intensity (EPI) and extreme precipitation frequency (EPF). For the extreme precipitation intensity, both positive and negative correlations could be found in many stations in the MLR-YR. Furthermore, the correlation coefficients between maximum NDVI and extreme precipitation intensity varied between  $-0.51$  and  $0.45$  among the 97 stations. For the extreme precipitation frequency, the correlation was smaller than that of extreme precipitation intensity. Concretely, correlation coefficients between extreme precipitation frequency and maximum NDVI varied between  $-0.41$  and  $0.41$ .

To elucidate spatial details of the positive and negative correlations, spatial heterogeneity of the correlations was analyzed to match changes in extreme precipitation events with that of the vegetation activity in the MLR-YR. Figure 4b,c show the spatial distribution of the correlations between maximum NDVI and EPI/EPF, respectively. The relationships between extreme precipitation events and vegetation activity was analyzed according to three groups of regions: weakened extreme precipitation events, enhanced extreme precipitation events and no obvious trends in extreme precipitation events.

In the regions with weakened extreme precipitation intensity but increasing extreme precipitation frequency, the correlations were mainly negative between extreme precipitation intensity and maximum NDVI in the MLR-YR over the period 1982–2012. This is especially obvious in the Hanjiang River Basin and the Dongting-Changjiang and the Poyang-Changjiang regions. This phenomenon means that weakened extreme precipitation intensity could ease the stress on vegetation activity. Furthermore, this occurred mainly in the regions with obvious changes in extreme precipitation events at a local scale.

In addition, obvious negative correlations could be found between extreme precipitation intensity and the maximum NDVI around the Chaohu-Changjiang region and around Sichuan Basin, where the intensity and frequency of extreme precipitation events were strengthened in past decades. However, positive correlations were also found between extreme precipitation intensity and the maximum NDVI, including places around the Danjiangkou Reservoir and in the northern parts of Chaohu Lake. This was especially obvious when extreme precipitation intensity increased but extreme precipitation frequency decreased.

When changes in the intensity/frequency of extreme precipitation events were relatively small or even lacking in obvious trends, both positive and negative correlations could be found between extreme precipitation intensity/frequency and maximum NDVI variables in the regions. This result indicates the uncertainty of weak extreme precipitation events on vegetation activity.

#### 4.3. Changes in Precipitation Extremes at Different Return Periods

Figure 5 shows precipitation extremes at the return periods of 30 years, 50 years and 100 years using GPD fitting in the MLR-YR during 1981–2012. Similar patterns of

daily precipitation extremes could be found in different return periods. However, obvious spatial heterogeneities exist among all three results. For example, maximum precipitation was concentrated in the eastern parts of the MLR-YR. Despite the increasing precipitation amounts with the increase of return periods, the rate of precipitation amounts is found to be spatially different in the MLR-YR. For instance, daily precipitation amount can reach 150 mm around the eastern Sichuan Basin in the western MLR-YR according to the results of the 30-year return period. Furthermore, the precipitation amounts can reach 210 mm for the return periods of 50 years and 100 years. In addition, the extent of precipitation extremes increases with the increasing return period. Similar phenomena could be found around the Poyang Lake and Dongting Lake in the middle and eastern MLR-YR. In contrast, changes in precipitation amount could be small in different return periods in many other regions.

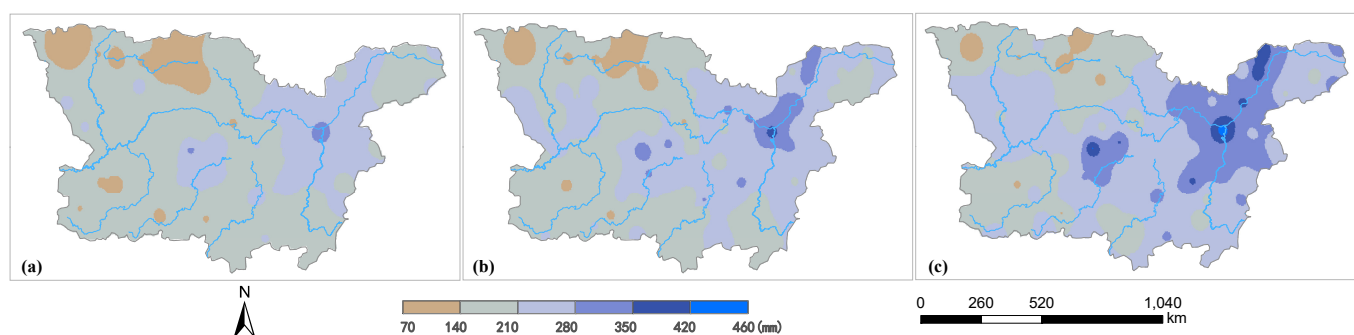


**Figure 5.** Daily precipitation extremes for different return periods: (a) 30 years; (b) 50 years; (c) 100 years.

## 5. Discussion

### 5.1. Relationship between Extreme Precipitation Events and Vegetation Activity

By taking the MLR-YR as a whole, with extreme precipitation frequency increased but slight changes in extreme precipitation intensity, maximum NDVI mainly shows increasing trends in most parts of the MLR-YR. According to further analysis of the spatial heterogeneity of the correlations, negative correlations (i.e., enhanced vegetation activity) could be found between extreme precipitation intensity and maximum NDVI under the condition of weakened extreme precipitation intensity but increasing extreme precipitation frequency in the past decades. This phenomenon could be associated with the abundant precipitation in the summer from weak but frequent occurrence of extreme precipitation events as well as the time-lag effects of vegetation responses to climate extremes [57]. The cumulative soil moisture from extreme precipitation events is beneficial to vegetation growth. The result is in accordance with soil moisture simulation [58].

However, when extreme precipitation intensity was strengthened, both positive and negative correlations could be found between extreme precipitation intensity and the maximum NDVI. This phenomenon means that vegetation responses may be different in line with changes in both the intensity and frequency of the extreme precipitation events. This phenomenon could be associated with the local severe impacts of extreme precipitation events on vegetation activity [28].

Many past studies have analyzed the relationships between extreme precipitation events and vegetation activity from the perspective of intensity and frequency of precipitation extremes. The relationships were frequently found to be conflicted between extreme precipitation events and vegetation activity [20,22–24]. This study analyzed their relationship by linking the frequency and intensity of extreme climate events simultaneously. This indicates a necessity to pay more attention to the combined effects of the frequency and intensity of extreme climate events when assessing impacts on vegetation activity [59,60].

### 5.2. Vegetation-Type-Based Analysis of the Relationship between Extreme Precipitation Events and Vegetation Activity

As shown above, the differences in the intensity/frequency of extreme precipitation events could have dramatic effects on vegetation activity, probably owing to the local occurrence of extreme precipitation events, the cumulative soil moisture from weak extreme precipitation, and the time-lag effects of vegetation responses. Besides these factors, vegetation types can play a critical role in such effects of extreme precipitation events [61,62]. According to our results, negative correlations could be found in the croplands in most regions of the MLR-YR, according to both the analysis of extreme precipitation frequency and extreme precipitation intensity (Figure 6). This negative correlation could be associated with the vulnerability of crop vegetation to precipitation extremes [63,64]. In the forest lands, different correlations were revealed as compared to croplands. Concretely, both positive and negative correlations could be found, not only for the extreme precipitation frequency but also for the extreme precipitation intensity. This uncertainty of the correlations could be associated with the moisture cumulative effect of the forest lands as well as the lag effect of the forest vegetation rather than the instantaneous effect as compared to crop vegetation [65,66]. These findings show that extreme precipitation events could have larger impacts on agricultural systems than forest types of vegetation.

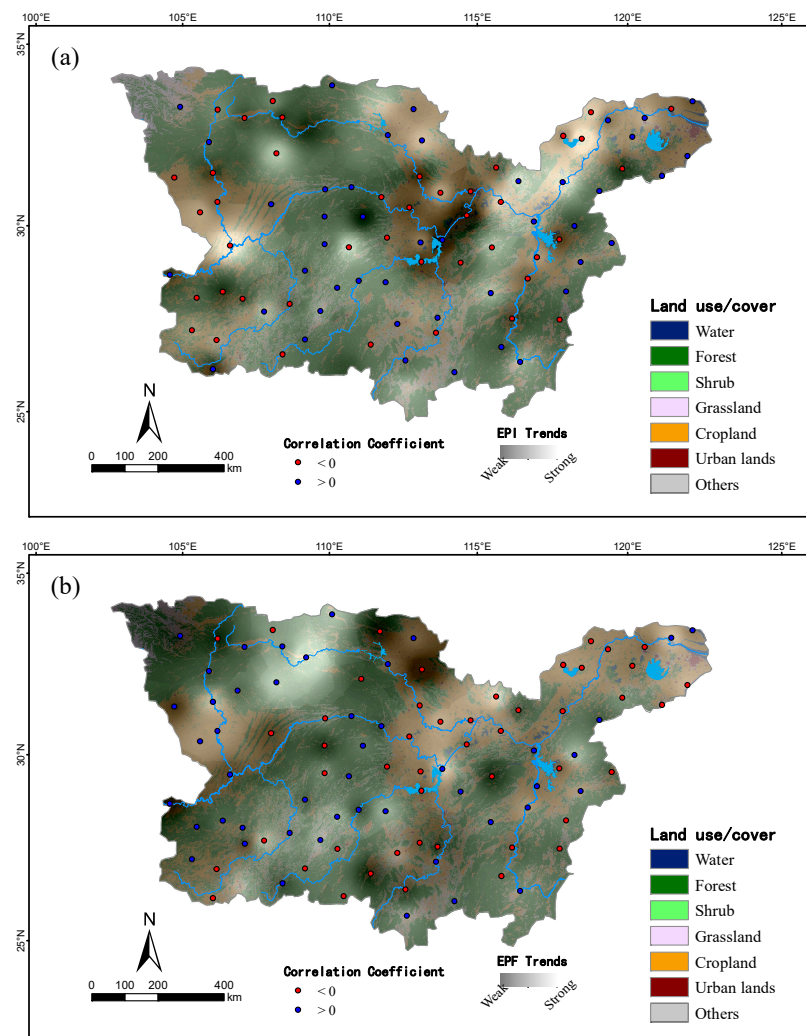


**Figure 6.** Vegetation-type-based analysis of the correlations between maximum NDVI and (a) extreme precipitation intensity and (b) extreme precipitation frequency.

### 5.3. Potential Risks of Extreme Precipitation Events on Vegetation Activity

A scientific understanding of the trends of climate extremes is important for assessing the potential risks of extreme precipitation events on vegetation activity. Huang et al. (2021) [67] found that eastern Asia, especially the MLR-YR, will experience moderate or high risks in the future, by combining historical daily precipitation and future daily projections from general circulation models (GCMs). However, the data resolution of the study of Huang et al. (2021) is relatively coarse, about  $1^\circ \times 1^\circ$ , and it should be further analyzed. In particular, it is crucial to study the trends in precipitation extremes and return levels [68–70]. This paper analyzed the potential risk of extreme precipitation events on vegetation activity by combining return period analysis and trend analysis of extreme precipitation events. We found that intensity and frequency of extreme precipitation events revealed an enhanced trend in the northeastern and western parts of the MLR-YR, such as around Chaohu Lake and Sichuan Basin, over the historical period of 1982–2012 (Figures 2 and 4). Despite this, return period analysis reveals slowing and slight increases. In addition, the intensity of extreme precipitation events was enhanced in the northern MLR-YR during 1982–2012, such as around the Danjiangkou-Hanjiang region. However, daily extreme precipitation amounts during a given return period were almost unchanged from 30-year to 100-year return periods. These differences revealed large risks of daily extreme precipitation events on the vegetation activity in these regions. The results are consistent with the findings of Huang et al. (2021) [67]. Furthermore, local occurrences of extreme precipitation events as well as their risks were also obvious according to our study. Thus, there is a potential risk to vegetation activity from strengthening extreme precipitation events in future decades.

## 6. Conclusions

In this paper, the impacts of extreme precipitation events on vegetation activity were analyzed using the MLR-YR as a case study. Key findings are as follows. (1) Taking the MLR-YR as a whole, both extreme precipitation events and vegetation activity were enhanced on average in the MLR-YR from 1982 to 2012. (2) Spatially, both positive and negative correlations could be found between maximum NDVI and extreme precipitation events in different stations in the MLR-YR. More attention should be paid from both perspectives of the frequency and intensity of extreme precipitation events simultaneously. (3) Such phenomena could be associated with the local occurrence of extreme precipitation events, the cumulative effects of soil moisture content from extreme precipitation events on vegetation growth rather than instantaneous effects at regional scale, as well as the difference in land cover types. (4) By coupling historical data analysis and return period analysis, the potential risks of extreme precipitation events on vegetation activity were identified in the Danjiangkou-Hanjiang area, around the eastern Sichuan Basin and around Chaohu Lake in the MLR-YR.

The objective of this paper is to explore the impacts of extreme precipitation events on vegetation activity. To better reflect spatiotemporal dependence of the extremes, the Bayesian hierarchical model will be tested in our future work to capture the changes in precipitation extremes as well as their impacts on vegetation activity [71,72]. In addition, our analysis was spatially conducted by interpolating observed precipitation records from 97 meteorological stations. The accuracy of the regional precipitation distributions is therefore limited in capturing the spatial heterogeneity of extreme precipitation events and their effects on vegetation activity. In future studies, precipitation data from remote sensing will be employed by comparing observed records from meteorological stations with independent proof of satellite-derived precipitation observations (e.g., TRMM 3B43 dataset).

**Author Contributions:** F.P. and Y.X. contributed to research design, data analysis, interpretation of results, and draft manuscript preparation; Y.Z. and F.P. contributed to the data collection; Y.Z. performed experiments and computational analysis; F.P. and Y.Z. drafted the paper. All authors



contributed to the final draft of the manuscript. All authors have read and agreed to the published version of the manuscript.

**Funding:** This research was funded by Qinglan Project of Jiangsu Province in China, the Project of Philosophy and Social Science Research in Colleges and Universities in Jiangsu Province (Grant No. 2019SJA0915), and the Priority Academic Program Development of Jiangsu Higher Education Institutions.

**Informed Consent Statement:** Not applicable.

**Data Availability Statement:** The datasets in this study are available within this article. The data that were derived from the original datasets but not included herein are available upon request.

**Acknowledgments:** The authors would like to thank the three anonymous reviewers for their insightful comments and suggestions.

**Conflicts of Interest:** The authors declare no conflict of interest.

## References

- Hansen, E.J.; Ruedy, R.; Sato, M.; Lo, K. Global surface temperature change. *Rev. Geophys.* **2010**, *48*, 4004. [CrossRef]
- Hansen, J.; Sato, M.; Ruedy, R.; Schmidt, G.A.; Lo, K.; Persin, A. Global Temperature in 2015. GISS, NASA, NY. 2016. Available online: <http://data.giss.nasa.gov> (accessed on 8 May 2020).
- IPCC. Summary for Policymakers. In *Climate Change and Land: An IPCC Special Report on Climate Change, Desertification, Land Degradation, Sustainable Land Management, Food Security, and Greenhouse Gas Fluxes in Terrestrial Ecosystems*; IPCC: Geneva, Switzerland, 2019.
- IPCC. Summary for Policymakers. In *Climate Change 2013: The Physical Science Basis. Contribution of Working Group I to the Fifth Assessment Report of the Intergovernmental Panel on Climate Change*; Stocker, T.F., Qin, D., Plattner, G.-K., Tignor, M., Allen, S.K., Boschung, J., Nauels, A., Xia, Y., Bex, V., Midgley, P.M., Eds.; Cambridge University Press: Cambridge, UK; New York, NY, USA, 2013.
- Cai, W.; Borlace, S.; Lengaigne, M.; Van Rensch, P.; Collins, M.; Vecchi, G.; Timmermann, A.; Santoso, A.; McPhaden, M.J.; Wu, L.; et al. Increasing frequency of extreme El Niño events due to greenhouse warming. *Nat. Clim. Chang.* **2014**, *4*, 111–116. [CrossRef]
- AghaKouchak, A.; Chiang, F.; Huning, L.S.; Love, C.A.; Mallakpour, I.; Mazdiyasn, O.; Moftakhari, H.; Papalexiou, S.M.; Ragno, E.; Sadegh, M. Climate Extremes and Compound Hazards in a Warming World. *Annu. Rev. Earth Planet. Sci.* **2020**, *48*, 519–548. [CrossRef]
- IPCC. *Managing the Risks of Extreme Events and Disasters to Advance Climate Change Adaptation: Special Report of the Intergovernmental Panel on Climate Change*; Field, C.B., Barros, V., Stocker, T.F., Qin, D., Dokken, D.J., Ebi, K.L., Mastrandrea, M.D., Mach, K.J., Plattner, G.K., Allen, S.K., et al., Eds.; Cambridge University Press: Cambridge, UK; New York, NY, USA, 2013; pp. 1–19.
- Mudelsee, M. *Statistical Analysis of Climate Extremes*; Cambridge University Press (CUP): Cambridge, UK, 2020.
- Pei, F.; Li, X.; Liu, X.; Lao, C. Assessing the impacts of droughts on net primary productivity in China. *J. Environ. Manag.* **2013**, *114*, 362–371. [CrossRef]
- Frank, D.; Reichstein, M.; Bahn, M.; Thonicke, K.; Frank, D.; Mahecha, M.; Smith, P.; van der Velde, M.; Vicca, S.; Babst, F.; et al. Effects of climate extremes on the terrestrial carbon cycle: Concepts, processes and potential future impacts. *Glob. Chang. Biol.* **2015**, *21*, 2861–2880. [CrossRef]
- Pei, F.; Wu, C.; Liu, X.; Li, X.; Yang, K.; Zhou, Y.; Wang, K.; Xu, L.; Xia, G. Monitoring the vegetation activity in China using vegetation health indices. *Agric. For. Meteorol.* **2018**, *248*, 215–227. [CrossRef]
- Felton, A.J.; Smith, M.D. Integrating plant ecological responses to climate extremes from individual to ecosystem levels. *Philos. Trans. R. Soc. B Biol. Sci.* **2017**, *372*, 20160142. [CrossRef]
- Yao, J.; Chen, Y.; Zhao, Y.; Mao, W.; Xu, X.; Liu, Y.; Yang, Q. Response of vegetation NDVI to climatic extremes in the arid region of Central Asia: A case study in Xinjiang, China. *Theor. Appl. Clim.* **2018**, *131*, 1503–1515. [CrossRef]
- Tovar, C.; Infantas, E.S.; Roth, V.T. Plant community dynamics of lomas fog oasis of Central Peru after the extreme precipitation caused by the 1997–98 El Niño event. *PLoS ONE* **2018**, *13*, e190572. [CrossRef] [PubMed]
- Piao, S.; Nan, H.; Huntingford, C.; Ciais, P.; Friedlingstein, P.; Sitch, S.; Chen, A. Evidence for a weakening relationship between interannual temperature variability and northern vegetation activity. *Nat. Commun.* **2014**, *5*, 1–7. [CrossRef] [PubMed]
- Jiapaer, G.; Liang, S.; Yi, Q. Vegetation dynamics and responses to recent climate change in Xinjiang using leaf area index as an indicator. *Ecol. Indic.* **2015**, *58*, 64–76.
- Gao, M.; Piao, S.; Chen, A.; Yang, H.; Liu, Q.; Fu, Y.H.; Janssens, I.A. Divergent changes in the elevational gradient of vegetation activities over the last 30 years. *Nat. Commun.* **2019**, *10*, 1–10. [CrossRef] [PubMed]
- Frich, P.; Alexander, L.V.; Della-Marta, P.; Gleason, B.; Haylock, M.; Tank, A.M.G.K.; Peterson, T. Observed coherent changes in climatic extremes during the second half of the twentieth century. *Clim. Res.* **2002**, *19*, 193–212. [CrossRef]
- Alexander, L.V. Global observed long-term changes in temperature and precipitation extremes: A review of progress and limitations in IPCC assessments and beyond. *Weather Clim. Extrem.* **2016**, *11*, 4–16. [CrossRef]

20. Tan, Z.; Tao, H.; Jiang, J.; Zhang, Q. Influences of Climate Extremes on NDVI (Normalized Difference Vegetation Index) in the Poyang Lake Basin, China. *Wetlands* **2015**, *35*, 1033–1042. [[CrossRef](#)]
21. Cui, L.; Wang, L.; Qu, S.; Singh, R.P.; Lai, Z.; Yao, R. Spatiotemporal extremes of temperature and precipitation during 1960–2015 in the Yangtze River Basin (China) and impacts on vegetation dynamics. *Theor. Appl. Clim.* **2018**, *136*, 675–692. [[CrossRef](#)]
22. Zhao, A.; Zhang, A.; Liu, X.; Cao, S. Spatiotemporal changes of normalized difference vegetation index (NDVI) and response to climate extremes and ecological restoration in the Loess Plateau, China. *Theor. Appl. Clim.* **2018**, *132*, 555–567. [[CrossRef](#)]
23. Felton, A.J.; Zavislan-Pullaro, S.; Smith, M.D. Semiarid ecosystem sensitivity to precipitation extremes: Weak evidence for vegetation constraints. *Ecology* **2018**, *100*, e2572. [[CrossRef](#)]
24. Luo, M.; Sa, C.; Meng, F.; Duan, Y.; Liu, T.; Bao, Y. Assessing extreme climatic changes on a monthly scale and their implications for vegetation in Central Asia. *J. Clean. Prod.* **2020**, *271*, 122396. [[CrossRef](#)]
25. Fisher, R.A.; Tippett, L.H.C. Limiting forms of the frequency distribution of the largest or smallest member of a sample. In *Proceedings of the Mathematical Cambridge Philosophical Society*; Cambridge University Press (CUP): Cambridge, UK, 1928; Volume 24, pp. 180–190.
26. Faranda, D.; Lucarini, V.; Turchetti, G.; Vaienti, S. Numerical convergence of the block-maxima approach to the generalized extreme value distribution. *J. Stat. Phys.* **2011**, *145*, 1156–1180. [[CrossRef](#)]
27. Lazoglou, G.; Anagnostopoulou, C.; Tolika, K.; Kolyva-Machera, F. A review of statistical methods to analyze extreme precipitation and temperature events in the Mediterranean region. *Theor. Appl. Clim.* **2018**, *136*, 99–117. [[CrossRef](#)]
28. Pei, F.; Wu, C.; Qu, A.; Xia, Y.; Wang, K.; Zhou, Y. Changes in Extreme Precipitation: A Case Study in the Middle and Lower Reaches of the Yangtze River in China. *Water* **2017**, *9*, 943. [[CrossRef](#)]
29. Zong, Y.; Chen, X. The 1998 Flood on the Yangtze, China. *Nat. Hazards* **2000**, *22*, 165–184. [[CrossRef](#)]
30. Shen, H.; Kuang, Y.; Li, Z.I. *Genesis of 2010 Storm-Flood in Yangtze River Basin and Its Comparison with 1998 Flood*; Yangtze River: Wuhan, China, 2011; Volume 42, pp. 11–14. (In Chinese)
31. China Meteorological Administration (CMA). *Surface Meteorological Observation Standards*; China Meteorological Press: Beijing, China, 1979.
32. National Center for Atmospheric Research Staff (NCAR). Last Modified 15 Mar 2018. The Climate Data Guide: NDVI: Normalized Difference Vegetation Index-3rd Generation: NASA/GFSC GIMMS. Available online: <https://climatedataguide.ucar.edu/climate-data/ndvi-normalized-difference-vegetation-index-3rd-generation-nasagfsc-gimms> (accessed on 24 May 2021).
33. Jordan, C.F. Derivation of leaf-area index from quality of light on the forest floor. *Ecology* **1969**, *50*, 663–666. [[CrossRef](#)]
34. Rouse, J.W., Jr.; Haas, R.; Schell, J.; Deering, D. *Monitoring Vegetation Systems in the Great Plains with ERTS*; NASA Special Publication: Washington, DC, USA, 1974; Volume 351, p. 309.
35. Tucker, C.J. Red and Photographic Infrared Linear Combinations for Monitoring Vegetation. *Remote Sens. Environ.* **1979**, *8*, 127–150. [[CrossRef](#)]
36. Kaufman, Y.J.; Tanre, D. Atmospherically resistant vegetation index (ARVI) for EOS-MODIS. *IEEE Trans. Geosci. Remote Sens.* **1992**, *30*, 261–270. [[CrossRef](#)]
37. Pei, F.; Zhou, Y.; Xia, Y. Application of Normalized Difference Vegetation Index (NDVI) for the Detection of Extreme Precipitation Change. *Forests* **2021**, *12*, 594. [[CrossRef](#)]
38. Pickands, J., III. Statistical inference using extreme order statistics. *Ann. Stat.* **1975**, *3*, 119–131.
39. Davison, A.C.; Smith, R.L. Models for Exceedances over High Thresholds. *J. R. Stat. Soc. Ser. B (Methodol.)* **1990**, *52*, 393–425. [[CrossRef](#)]
40. Wang, Q. The POT model described by the generalized Pareto distribution with Poisson arrival rate. *J. Hydrol.* **1991**, *129*, 263–280. [[CrossRef](#)]
41. Acero, F.J.; García, J.A.; Gallego, M.C. Peaks-over-threshold study of trends in extreme rainfall over the Iberian Peninsula. *J. Clim.* **2011**, *24*, 1089–1105. [[CrossRef](#)]
42. Pandey, M.; Van Gelder, P.; Vrijling, J. The estimation of extreme quantiles of wind velocity using L-moments in the peaks-over-threshold approach. *Struct. Saf.* **2001**, *23*, 179–192. [[CrossRef](#)]
43. Thiombiano, A.N.; El Adlouni, S.; St-Hilaire, A.; Ouarda, T.B.; El-Jabi, N. Nonstationary frequency analysis of extreme daily precipitation amounts in Southeastern Canada using a peaks-over-threshold approach. *Theor. Appl. Clim.* **2017**, *129*, 413–426. [[CrossRef](#)]
44. Karl, T.R.; Nicholls, N.; Ghazi, A. Clivar/GCOS/WMO workshop on indices and indicators for climate extremes workshop 549 summary. In *Weather and Climate Extremes*; Springer: Berlin/Heidelberg, Germany, 1999; pp. 3–7.
45. Kim, J.; Jain, S. Precipitation trends over the Korean peninsula: Typhoon-induced changes and a typology for characterizing climate-related risk. *Environ. Res. Lett.* **2011**, *6*, 34033. [[CrossRef](#)]
46. Villarini, G.; Smith, J.A.; Baeck, M.L.; Vitolo, R.; Stephenson, D.B.; Krajewski, W.F. On the frequency of heavy rainfall for the Midwest of the United States. *J. Hydrol.* **2011**, *400*, 103–120. [[CrossRef](#)]
47. Villarini, G.; Smith, J.A.; Vecchi, G.A. Changing Frequency of Heavy Rainfall over the Central United States. *J. Clim.* **2013**, *26*, 351–357. [[CrossRef](#)]
48. Elquliti, S.; Alfalatah, S.M.; Alghamdi, M.; Alabdali, Y.; Ahmed, A. Assessment of the Frequency and Return Period for Extreme rainfall Causing Floods Inmecca, Saudi Arabia. *Int. J. Sci. Technol. Res. Eng.* **2016**, *1*, 1–5.

49. Deidda, R.; Puliga, M. Performances of some parameter estimators of the generalized Pareto distribution over rounded-off samples. *Phys. Chem. Earth Parts A/B/C* **2009**, *34*, 626–634. [[CrossRef](#)]
50. Hosking, J.R. L-moments analysis and estimation of distributions using linear combinations of order statistics. *J. R. Stat. Soc. Ser. B (Methodol.)* **1990**, *52*, 105–124. [[CrossRef](#)]
51. Palutikof, J.P.; Brabson, B.B.; Lister, D.H.; Adcock, S.T. A review of methods to calculate extreme wind speeds. *Meteorol. Appl.* **1999**, *6*, 119–132. [[CrossRef](#)]
52. Santos, E.B.; Lucio, P.S.; Silva, C.M.S. Estimating return periods for daily precipitation extreme events over the Brazilian Amazon. *Theor. Appl. Climatol.* **2016**, *126*, 585–595. [[CrossRef](#)]
53. Jenkinson, A.F. The frequency distribution of the annual maximum (or minimum) values of meteorological elements. *Q. J. R. Meteorol. Soc.* **2010**, *81*, 158–171. [[CrossRef](#)]
54. R Core Team. *R: A Language and Environment for Statistical Computing*; R Foundation for Statistical Computing: Vienna, Austria, 2016. Available online: <https://www.R-project.org/> (accessed on 15 May 2021).
55. Gilleland, E.; Katz, R.W. extRemes2.0: An Extreme Value Analysis Package in R. *J. Stat. Softw.* **2016**, *72*, 1–39. [[CrossRef](#)]
56. Ribatet, M.; Dutang, C. A User's Guide to the POT Package (Version 1.0). 2016. Available online: <http://cran.r-project.org/> (accessed on 24 May 2021).
57. Wu, D.; Zhao, X.; Liang, S.; Zhou, T.; Huang, K.; Tang, B.; Zhao, W. Time-lag effects of global vegetation responses to climate change. *Glob. Chang. Biol.* **2015**, *21*, 3520–3531. [[CrossRef](#)] [[PubMed](#)]
58. Mimeau, L.; Trambly, Y.; Brocca, L.; Massari, C.; Camici, S.; Finaud-Guyot, P. Modeling the response of soil moisture to climate variability in the Mediterranean region. *Hydrol. Earth Syst. Sci.* **2021**, *25*, 653–669. [[CrossRef](#)]
59. Gessner, U.; Naeimi, V.; Klein, I.; Kuenzer, C.; Klein, D.; Dech, S. The relationship between precipitation anomalies and satellite-derived vegetation activity in Central Asia. *Glob. Planet. Chang.* **2013**, *110*, 74–87. [[CrossRef](#)]
60. Leathers, D.J.; Brasher, S.E.; Brinson, K.R.; Hughes, C.; Weiskopf, S. A comparison of extreme precipitation event frequency and magnitude using a high-resolution rain gage network and NOAA Atlas 14 across Delaware. *Int. J. Clim.* **2020**, *40*, 3748–3756. [[CrossRef](#)]
61. Li, C.; Wang, J.; Hu, R.; Yin, S.; Bao, Y.; Ayal, D.Y. Relationship between vegetation change and extreme climate indices on the Inner Mongolia Plateau, China, from 1982 to 2013. *Ecol. Indic.* **2018**, *89*, 101–109. [[CrossRef](#)]
62. Islam, A.R.M.T.; Islam, H.; Shahid, S.; Khatun, M.K.; Ali, M.M.; Rahman, M.; Ibrahim, S.M.; Almoajel, A.M. Spatiotemporal nexus between vegetation change and extreme climatic indices and their possible causes of change. *J. Environ. Manag.* **2021**, *289*, 112505. [[CrossRef](#)]
63. Lal, M.; Singh, K.; Rathore, L.; Srinivasan, G.; Saseendran, S. Vulnerability of rice and wheat yields in NW India to future changes in climate. *Agric. For. Meteorol.* **1998**, *89*, 101–114. [[CrossRef](#)]
64. Zheng, H.; Shen, G.; He, X.; Yu, X.; Ren, Z.; Zhang, D. Spatial assessment of vegetation vulnerability to accumulated drought in Northeast China. *Reg. Environ. Chang.* **2015**, *15*, 1639–1650. [[CrossRef](#)]
65. Savage, J.; Vellend, M. Elevational shifts, biotic homogenization and time lags in vegetation change during 40 years of climate warming. *Ecography* **2015**, *38*, 546–555. [[CrossRef](#)]
66. Wen, Y.; Liu, X.; Pei, F.; Li, X.; Du, G. Non-uniform time-lag effects of terrestrial vegetation responses to asymmetric warming. *Agr. For. Meteorol.* **2018**, *252*, 130–143. [[CrossRef](#)]
67. Huang, H.; Cui, H.; Ge, Q. Assessment of potential risks induced by increasing extreme precipitation under climate change. *Nat. Hazards* **2021**, 1–21. [[CrossRef](#)]
68. Fernández, B.; Salas, J.D. Return Period and Risk of Hydrologic Events. I: Mathematical Formulation. *J. Hydrol. Eng.* **1999**, *6*, 297–307. [[CrossRef](#)]
69. Fernández, B.; Salas, J.D. Return Period and Risk of Hydrologic Events. II: Applications. *J. Hydrol. Eng.* **1999**, *4*, 308–316. [[CrossRef](#)]
70. Chen, Y.R.; Chu, P.-S. Trends in precipitation extremes and return levels in the Hawaiian Islands under a changing climate. *Int. J. Clim.* **2014**, *34*, 3913–3925. [[CrossRef](#)]
71. Ghosh, S.; Mallick, B.K. A hierarchical Bayesian spatio-temporal model for extreme precipitation events. *Environmetrics* **2011**, *22*, 192–204. [[CrossRef](#)]
72. Sharkey, P.; Winter, H.C. A Bayesian spatial hierarchical model for extreme precipitation in Great Britain. *Environmetrics* **2019**, *30*, e2529. [[CrossRef](#)]